Ti *K*-edge XANES studies of Ti coordination and disorder in oxide compounds: Comparison between theory and experiment

François Farges*
Laboratoire de Physique et Mécanique des Géomatériaux, Université de Marne-la-vallée (and UA CNRS 734 and LURE), 93166 Noisy le Grand cedex, France

Gordon E. Brown, Jr.
Department of Geological and Environmental Sciences and Stanford Synchrotron Radiation Laboratory, Stanford University, Stanford, California 94305-2115

J. J. Rehr
Department of Physics, University of Washington, Seattle, Washington 98195
(Received 11 November 1996)

Experimental Ti *K*-edge x-ray-absorption near-edge structure (XANES) spectra for a variety of Ti(IV)-bearing crystalline oxide model compounds are compared with those calculated using the *ab initio* multiple-scattering code FEFF7. A scattering-theoretic interpretation of various features in the experimental spectra, including pre-edge and main-edge peaks, is presented together with an interpretation of the effects of disorder. The observed pre-edge features are found to vary in both position (by $\approx 2 \pm 0.1$ eV) and normalized height (from ≈ 0.04 to 1.0 ± 0.05) as a function of Ti coordination (4, 5, or 6 oxygen nearest neighbors), in agreement with calculations. In aperiodic oxide compounds where the Ti coordination is unknown (e.g., titanosilicate glasses and melts), pre-edge position and height can be used to derive reliable information on Ti coordination chemistry. For example, one can distinguish between fivefold coordinated Ti (i.e., TiO_5) and a 50:50 mixture of fourfold- and sixfold-coordinated Ti (i.e., TiO_4 vs TiO_6). Finally, it is proposed that the intensity of the main-edge features can be used as a probe of disorder in the short- and medium-range environment of Ti. This is exemplified by Ti XANES studies of the effect of radiation damage on $CaTiSiO_5$ and the melting of $K_2TiSi_2O_7$ glass at high temperature. [S0163-1829(97)00927-2]

I. INTRODUCTION

Titanium *K*-edge x-ray-absorption near-edge structure (XANES) spectroscopy is widely used to derive information on the coordination environment of tetravalent Ti[Ti(IV)] in structurally complex oxide materials, such as titanosilicate glasses and melts.[1–4] However, a quantitative understanding of the influence of coordination and disorder on XANES spectra is lacking. In particular, the height of Ti pre-*K*-edge features has been shown to be related to the geometry of Ti-oxygen polyhedra, particularly Ti coordination number.[1–5] However, a quantitative understanding of the influence of coordination and disorder on XANES spectra is lacking. Many previous Ti XANES studies have focused on oxide and silicate compounds in which Ti(IV) is fourfold or sixfold coordinated,[1,5] whereas Ti-bearing silicate glasses contain significant amounts of fourfold and fivefold coordinated Ti(IV).[1–4] All three Ti coordinations in aperiodic oxide-type materials can be detected using XANES only if the variation of the Ti pre-*K*-edge features as a function of Ti coordination is well understood. This can be accomplished through a combination of experiment and theory, involving collection of XANES spectra for a large set of well-characterized oxide model compounds representative of the coordination chemistry of Ti(IV) and theoretical simulations of such spectra to provide a quantitative understanding of their variations.

In this study, we report high-resolution Ti *K*-edge XANES spectra of a number of Ti model compounds in which Ti is located in sites coordinated by 4, 5 and or 6 oxygens. We also present *ab initio* XANES calculations for various Ti-bearing model compounds, made using the high-order multiple-scattering (MS) codes FEFF6 (Ref. 6) and FEFF7 (Ref. 7), which agree well with the observed spectra and provide a scattering-theoretic interpretation of the experimental spectra. We propose a method for determining Ti coordination numbers from pre-edge peak data that is based on the observed variation of pre-edge position and height as a function of Ti coordination. Our experimental observations suggest that the XANES region is highly sensitive to disorder in the short- and medium-range environment of Ti. A scattering-theoretic interpretation of these results together with a general discussion of the effects of disorder is also given. Finally, an application of these methods to crystalline, radiation-damaged, and glassy $CaTiSiO_5$ and to glassy and molten $K_2TiSi_2O_7$ is presented.

II. EXPERIMENT

The various Ti(IV)-bearing model compounds examined in this study are listed in Table I. More detailed information on their crystal structures and synthesis protocols can be found elsewhere.[4] These model compounds contain the Ti(IV) coordinations found in Ti-containing oxides and silicates, including fourfold, fivefold, and sixfold coordinated Ti(IV).

TABLE I. Pre-edge data for Ti-containing model compounds.

	Ti coordination	Pre-edge data			
		Position (ev)	Normalized height	FWHM (ev)	Peak area
$Ni_{2.6}Ti_{0.7}O_4$	4	4969.6	0.94	0.8	1.2
$Ni_{2.4}Ti_{0.7}Si_{0.05}O_4$	4	4969.5	0.60	1.1	1.0
β-Ba_2TiO_4	4	4969.4	1.00	0.8	1.2
α-Ba_2TiO_4	4	4969.5	1.00	0.8	1.2
$CsAlTiO_4$	4	4969.7	≈ 0.9[a]	≈ 0.8[a]	≈ 1[a]
Rb_2TiO_3	4	4969.6	1.00	0.8	1.2
$K_6Ti_2O_7$	4	4969.7	0.93	0.9	1.3
Y_2TiMoO_8	4	4969.9	0.74	0.9	1.0
Na_4TiO_4	4	4969.6	0.70	0.9	0.9
$KNaTiO_3$	5	4970.6	0.73	0.8	0.8
$Ba_2TiSi_2O_8$	5	4970.6	0.67	0.8	0.8
$Sr_2TiSi_2O_8$	5	4970.5	0.71	0.8	0.8
$Ba_2TiGe_2O_8$	5	4970.6	0.65	0.8	0.8
$Na_2Ti_4O_9$	5	4970.5	0.43	1.1	0.8
$K_2Ti_4O_9$	5	4970.6	0.45	1.1	0.8
$Rb_2Ti_4O_9$	5	4970.5	0.47	1.1	0.8
$K_2Ti_2O_5$	5	4970.6	0.51	1.1	0.8
r-TiO_2	6	4971.6	0.22	1.3	0.4
a-TiO_2	6	4971.5	0.17	1.3	0.3
$CaTiO_3$	6	4971.6	0.11	1.4	0.2
$BaTiSi_3O_9$	6	4971.2	0.04	1.4	0.1
$KNa_2LiFe_2Ti_2Si_8O_{24}$	6	4971.1	0.32	1.3	0.6
$FeTiO_3$	6	4971.7	0.22	1.4	0.5
$CaTiSiO_5$	6	4971.4	0.18	1.3	0.4
$TiZrO_4$	6	4971.1	0.21	1.3	0.4
$Ca_3(Ti,Zr)_2(Si,Al_2)O_{12}$	6	4971.2	0.15	1.3	0.3
Error		± 0.1	± 0.05	± 0.1	± 0.1

[a]These are estimates. More quantitative values are not possible because of interference from the Cs L_{III} edge.

Ti pre-edge and K-edge (4966 eV) spectra for model compounds were collected in the transmission mode at the LURE facility (Laboratoire pour l'Utilisation du Rayonnement Electromagnétique, Orsay, France) on beam station EXAFS4. The DCI storage ring was operating at 1.8 GeV and 100–300 positron current. A Si (311) double-crystal monochromator (detuned 60% to eliminate most of the higher-energy harmonics) and a 0.3-mm vertical slit (before the monochromator) were used to ensure high-resolution data (0.05-eV steps, energy resolution ≈ 1.2 eV at 5 keV.) The monochromator energy calibration was checked between each spectrum using a Ti metal foil to provide energy reproducibility of ± 0.05 eV in the experimental spectra. X-ray absorption fine structure (XAFS) data for all Ti model compounds were collected under a vacuum of 10^{-3} atm to minimize hydration. Helium gas was used in the incident beam ionization chamber, whereas the transmitted beam ionization chamber was filled with Ar gas. Samples were prepared by deposition of powders of these materials on kapton tape (thicknesses of 20–50 μm for an absorbance of $\mu \approx 2$ at 5 keV; the edge jump was between 0.5 and 1.5).

Pre-edges were normalized in absorbance by fitting the spectral region from 4850 to 4950 eV (the region below the pre-edge) using a Victoreen function and subtracting this as background absorption. The pre-edges were then normalized for atomic absorption, based on the average absorption coefficient of the spectral region from 5050 to 5200 eV (after the main-edge crest). Pre-edge information (absolute position, normalized height, half-width, and peak area, Table I) was extracted from the normalized pre-edge spectra by fitting Lorentzians to these features.

III. THEORETICAL CALCULATIONS

XANES spectra were calculated using the *ab initio* multiple-scattering code FEFF (Ref. 6) (versions 6 and 7), which we refer to as FEFF. This code is based on the multiple-scattering expansion in a system with spherical muffin-tin potentials and uses the extended continuum approximation to treat all XANES features in terms of the scattering of continuum photoelectrons, including those usually ascribed to bound electronic transitions. Such ''bound-state'' transitions (for example, the $1s \rightarrow 3d$ transition attributed to the pre-edge feature of Ti K XANES spectra) are represented in this formalism as continuum resonances that can be approximated by a suitably large number of scattering events along the same localized paths (e.g., the path of order 4 of a TiO_4 tetrahedron: Ti→O→Ti→O→Ti). Such a formalism

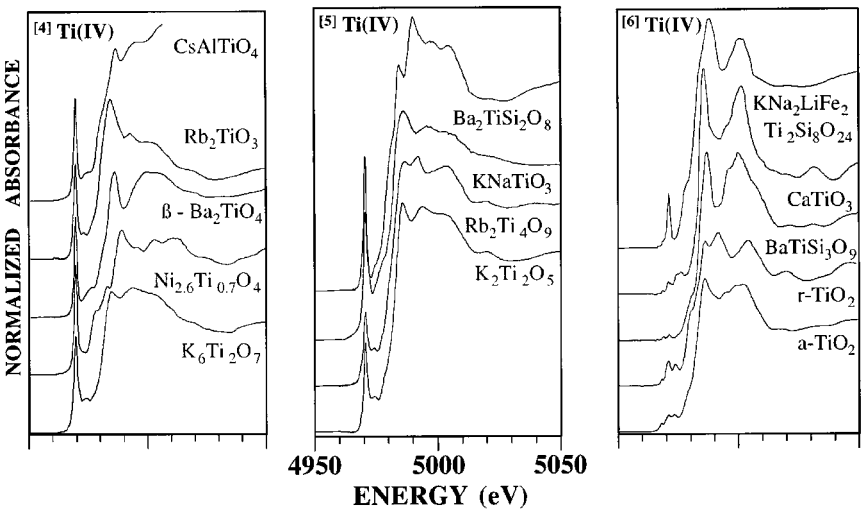

FIG. 1. Ti *K*-edge XANES spectra for selected Ti-crystalline oxide model compounds containing fourfold coordinated (left), fivefold coordinated (middle), and sixfold coordinated Ti (right).

can only represent sharp continuum resonances when the MS expansion converges rapidly and hence the method can fail when the broadening effects of core-hole lifetime, inelastic losses and Debye-Waller factors are all negligible, e.g., near the edge in low-Z materials such as Si. The high-order MS approach has several advantages compared to the full MS calculation, in particular, the ability to treat very large clusters over a large energy range, including disorder on a path-by-path basis. This approach can also identify the important geometrical paths that contribute to a specific feature, whereas it is difficult to make such attributions using a full MS approach. Remarkably, convergence of the MS expansion is often sufficiently rapid that this finite MS approach can provide a quantitative interpretation of edge-feature positions and strengths in a wide range of materials. The atomic cluster used to model the Ti *K* XANES spectrum and to simulate the important MS paths responsible for the XANES may be either a large cluster [e.g., $(TiO)O_4Si_4K_4$] or a small cluster embedded in a larger one [e.g., $(TiO)O_4$ in $(TiO)O_4Si_4K_4$]. The coordinates of atoms in each cluster are taken from crystal structures of Ti compounds derived from x-ray-diffraction data. In either case, the scattering potential is that of the larger cluster, which is chosen to be representative of the solid. We obtained the best results using the default Hedin-Lundqvist self-energy together with an added constant energy shift, with a real part of 4 eV and an imaginary part of 0.5 eV to account for the error in FEFF estimate of threshold E_0, which is based on the Fermi energy of a free-electron gas and instrumental broadening, respectively (''EXCHANGE 0 4 0.5'' option). All muffin-tin radii were automatically overlapped (by $\approx$20%; ''AFOLP'' option) to reduce the effects of discontinuities in their overlap regions and to give a better molecular potential for materials with highly inhomogeneous electron density distributions, which is appropriate for the compounds studied here. In addition, we have found it desirable to include in the calculations all MS paths up to order-8 scatterers, with a maximum effective path length of 7 Å (''CRITERION 0 0'' and ''RMAX 7'' options), rather than the usual path filters in FEFF, which ignore low-amplitude paths. The order of MS needed for convergence is roughly determined by the criterion that $\langle |f_{\rm eff}|\exp(ikR-R/\lambda)/kR\rangle$ is small, and hence is determined by the magnitude of scattering, mean free paths, and Debye-Waller factors. In practice, we have found that convergence is often better than that predicted by this estimate, possibly due to random phase cancellations between high-order MS paths. We found that the two options AFOLP and CRITERION 0 0 are crucial for calculating XANES spectra in these materials that agree quantitatively with the experimental spectra. We therefore suggest their use for other K and $L_{\rm III}$ edges (e.g., Cr, Co, Ni, Zr, Pt, U). Indeed, this finding suggests that much smaller cutoff criteria may be desirable for general XANES calculations, especially for aperiodic systems that lack significant path degeneracies. Default values for the Debye-Waller factors associated with each calculated path were used (i.e., zero) because of the absence of Debye-Einstein temperature information for the systems studied and the small effect of disorder on the absorption coefficient in the near-edge region. Thus, these calculations underestimate the broadening effects due to thermal and structural disorder and give extended fine structure (EXAFS) amplitudes that are too large compared with experiment. We discuss the effect of structural disorder on Ti *K* XANES spectra later in the paper.

The approach we have taken considers only MS involving short- and medium-range structure together with a carefully chosen potential. Construction of the potential, which includes choosing an appropriate molecular cluster without unphysical surface effects, and reduction of the effects of muffin-tin potential discontinuities and the errors due to the flat potential in the interstitial regions, are all crucial elements of the FEFF calculation. We feel that this step can be more important in successful simulations of near-edge and XANES spectra than consideration of MS for long paths. Intuition suggests that incoherent MS along most long paths will result in very low-amplitude spectral features, whereas coherent MS, e.g., from repeated paths, can be important. Furthermore, we know very little about the effects of disorder of long scattering paths that extend outside a cluster and, therefore, cannot accurately describe Debye-Waller factors for such paths in a full MS calculation. Ti in the model compounds and aperiodic oxides examined in this study is located in sites with short-range tetrahedral, square-pyramidal, or octahedral symmetry. Thus a calculation in which one considers only high-order MS in a small cluster, with the small cluster embedded in an appropriately chosen

larger cluster needed to accurately describe the potential, is both more efficient and more physically realistic than full MS of a large cluster.

IV. PRE-EDGE FEATURES IN Ti OXIDES

A. Fourfold, fivefold, and sixfold coordinated Ti in crystalline oxides

Figure 1 shows a selection of Ti K-edge spectra from model compounds in which Ti is located in sites coordinated by 4, 5, or 6 oxygens. The Ti pre-edge features are located $\approx 18 \pm 3$ eV before the main-edge crest. These features are commonly attributed to transitions from Ti $1s$ energy levels to bound Ti $3d$ (or O $2p$) molecular orbitals.[5,8,9] In this picture the transitions are discrete, with broadening due to core-hole lifetime and instrumental resolution. Here we discuss these spectra from an equivalent scattering-theoretic interpretation,[10] which is more like a band-structure approach where the molecular levels broaden into continuous energy bands. Indeed it has been shown that the MS expansion is equivalent to a Koringa-Kohn-Rostoker band-structure calculation, provided it converges.[11] The scattering-theoretic picture takes into account the self-energy of the photoelectron, which gives additional broadening due to the finite mean free path and also accounts for the effect of structural disorder on the near-edge spectra. Using this approach, most of the pre-edge behavior can be attributed to MS effects, since the atomiclike absorption from the central muffin-tin potential is smoothly varying above the muffin-tin potential zero. For Ti K-edge absorption, the destructive interference from the nearest-neighbor oxygens produces a large dip in the spectra just beyond threshold. Here we identify threshold as the Fermi energy (which is determined by overall charge neutrality) or the lowest unoccupied final state. The Fermi energy defines the onset of absorption, since absorption of x rays by electronic transitions to occupied final states is forbidden. Thus the Fermi energy lies below both the pre-edge and the main absorption edge. The dominant pre-edge peak (if any) arises from structure in the final-state p density (p-DOS) just beyond the Fermi energy. Its origin is likely due to mixing with the unoccupied narrow d-band states in the pre-edge region. In the Ti compounds discussed in this paper, the Fermi energy is pinned by these d states. Because of its narrow width, this pre-edge feature is analogous to a bound state. In the equivalent molecular orbital or ligand field description of this feature, mixing of d and p orbitals is possible when the absorbing atom is not on a center of symmetry, thus allowing this dipole transition. The pre-edge is therefore controlled by both the location of the Fermi energy and the nature of the p-DOS. One potentially confusing point in the comparison of band theory and molecular orbital descriptions of this ''bound state'' transition for insulating compounds like those we are considering is that the Fermi level lies at an energy just below the first pre-edge feature. It is possible to have quasilocalized states just above the Fermi level in which the electron is essentially bound, but which also allow the electron to hop from center to center and eventually escape to the continuum. Such quasilocalized states in the band theory description would correspond to bound states in the molecular orbital description.

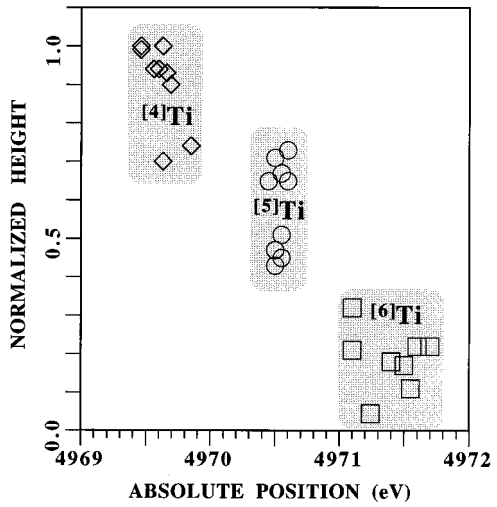

FIG. 2. Normalized pre-edge height vs energy position for Ti K-pre-edge features in model compounds listed on Table I showing three domains for fourfold, fivefold, and sixfold coordinated Ti.

As we discuss below, our scattering-theoretic interpretation can explain quantitatively the influence of coordination and disorder on pre-edge features (energy position and normalized height). In order to support this interpretation, we present a comparison between experimental and theoretical (i.e., MS FEFF simulated) pre-edge spectra.

In agreement with previous studies,[1,2,4,12] the experimental pre-edge features are found to have the greatest height for fourfold coordinated Ti, $^{[4]}$Ti model compounds (e.g., as high as 100% of the edge jump in $Rb_2{}^{[4]}TiO_3$ in our experiments), and they are shifted to lower energies by 2 eV compared to $^{[6]}$Ti coordination. For example, the pre-edge for β-$Ba_2{}^{[4]}TiO_4$ is shifted by -2.2 ± 0.1 eV compared to rutile

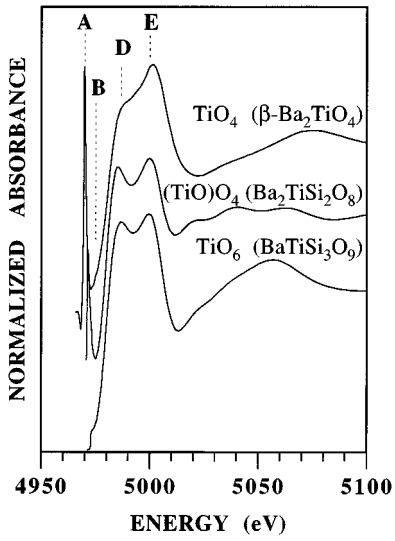

FIG. 3. Results of FEFF MS calculations of Ti K XANES spectra for $^{[4]}TiO_4$, $(^{[5]}TiO)O_4$, and $^{[6]}TiO_6$ units in β-$Ba_2{}^{[4]}TiO_4$, $Ba_2{}^{[5]}TiSi_2O_8$ and $Ba^{[6]}TiSi_3O_9$ model compounds, respectively, using paths of order $n \leq 8$. In each calculation, the small clusters were embedded in larger clusters representative of each crystal structure (see Table II).

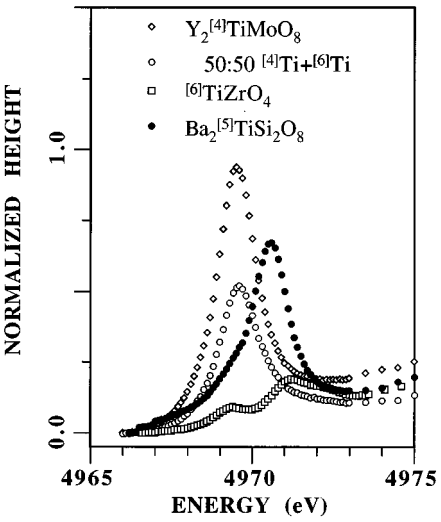

FIG. 4. Comparison of the measured pre-edge features in Ti *K* XANES spectra of $^{[4]}$Ti (as $Y_2{}^{[4]}TiMoO_4$), $^{[5]}$Ti (as $Ba_2{}^{[5]}TiSi_2O_8$), and $^{[6]}$Ti (as $^{[6]}TiZrO_4$) with a pre-edge spectrum simulating a 50:50 mixture of $^{[4]}$Ti and $^{[6]}$Ti (as $Y_2{}^{[4]}TiMoO_4$ and $^{[6]}TiZrO_4$, respectively).

(r-$^{[6]}TiO_2$). Pre-edge energies and heights for $^{[5]}$Ti model compounds fall between the values measured for the other two Ti coordinations, resulting in three well-separated $^{[4]}$Ti, $^{[5]}$Ti, and $^{[6]}$Ti domains in the plot of pre-edge energies versus pre-edge height (Fig. 2).

Ab initio FEFF XANES calculations were performed for typical TiO_4, TiO_5, and TiO_6 clusters found in selected Ti-model compounds (Fig. 3). These calculations are in general agreement with those of Paris and co-workers,[13] who used a full-MS code (CONTINUUM?). This agreement suggests that the paths approach of FEFF is a good approximation of full MS theory, at least for fourfold and fivefold coordinated Ti(IV) bearing oxides [see the rutile section below for a discussion of the case of sixfold coordinated Ti(IV)]. However, a major difference between the Paris *et al.* study and this one is that the present study is more successful in modeling the intense pre-edge feature for fivefold coordinated Ti in a square-pyramidal polyhedron, a result that is consistent with experiment (see Fig. 1; $KNaTiO_3$ or $Ba_2TiSi_2O_8$, which has Ti in such a geometry). Our calculations indicate that $^{[4]}$Ti has $\approx$2.5 times greater pre-edge height than $^{[5]}$Ti, which is in the same direction as that observed for model compounds but higher by $\approx +40\%$. These calculations also indicate that the pre-edge position is shifted toward higher energies by about $+2$ eV when the Ti coordination increases from 4 to 5, which is in the same direction (but slightly larger) as that observed for model compounds ($+0.8$ to $+1.1$ eV). The shift in pre-edge position appears to be associated with a shift in the Fermi energy with increasing coordination of the Ti. The differences between predicted and experimental pre-edge height and position are not unexpected given the broadening effect of the Ti core-hole width ($\approx$0.8 eV for the Ti *K* edge) plus instrumental factors (type and mosaic spread of the monochromator crystals, source size, slit heights, beam instabilities, etc.) and also uncertainties in the scattering potentials used in the calculations.

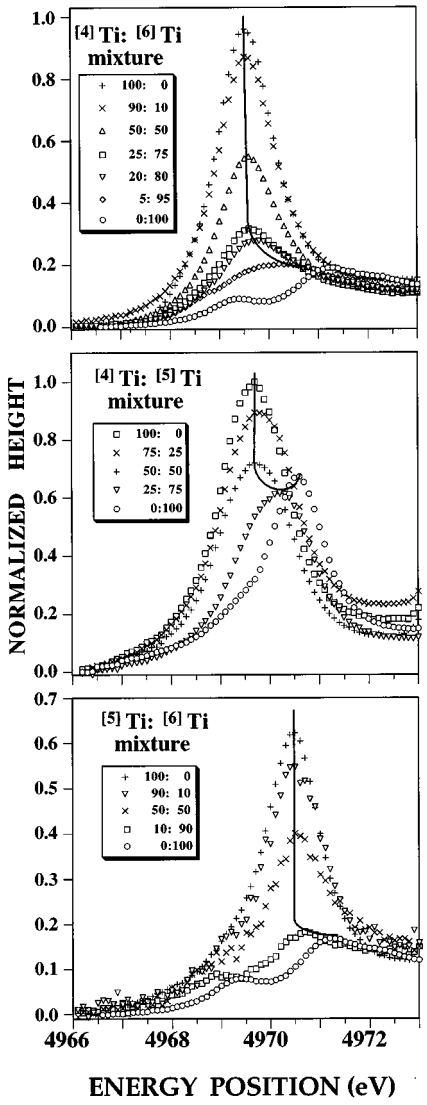

FIG. 5. Pre-edges collected for mixtures of Ti coordinations. Left: $^{[4]}$Ti and $^{[6]}$Ti assuming $Ni_{2.6}{}^{[4]}Ti_{0.7}O_4$ and $^{[6]}TiZrO_4$ end members; middle: $^{[4]}$Ti and $^{[5]}$Ti assuming $Y_2{}^{[4]}TiMoO_8$ and $Ba_2{}^{[5]}TiGe_2O_8$ end members; right: $^{[5]}$Ti and $^{[6]}$Ti assuming $Ba_2{}^{[5]}TiSi_2O_8$ and $^{[6]}CaTiSiO_5$ end members.

B. Pre-edge features for mixture of Ti coordinations

The use of either position or normalized peak height alone is not sufficient to derive reliable coordination numbers for Ti when it is present in several coordinations. A typical example of possible misinterpretation of pre-edge information is shown in Fig. 4. The pre-edge feature for a 50:50 mixture of $^{[4]}$Ti as $Y_2{}^{[4]}TiMoO_4$ and $^{[6]}$Ti as $^{[6]}TiZrO_4$ is located at 4969.9 eV, which is close to that for $^{[4]}$Ti and inconsistent with that expected for $^{[6]}$Ti, whereas its normalized height (0.56) suggests the presence of $^{[5]}$Ti. However, the pre-edge position is inconsistent with that for $^{[5]}$Ti. To understand these effects better, an extensive set of pre-edge spectra of mixtures of model compounds with fourfold, fivefold, and/or sixfold coordinated Ti was collected and compared to theoretical simulations (Fig. 5). Based on these results, a summary of pre-edge information for various mixtures of Ti coordinations is presented in Fig. 6. This survey suggests that if

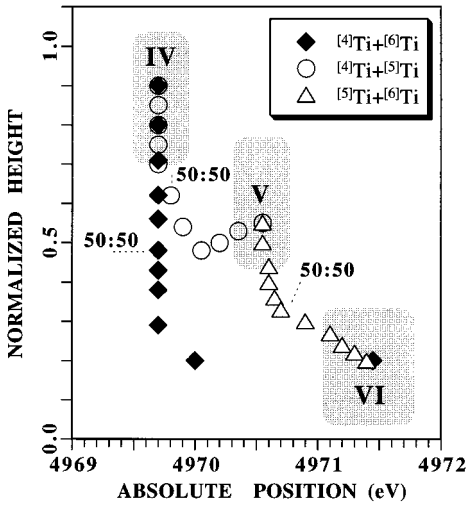

FIG. 6. Plot of normalized height vs energy of the Ti pre-edge feature showing the predicted values for different mixtures between fourfold, fivefold, and sixfold coordinated Ti.

one considers only the pre-edge position, an underestimation of Ti coordination number is likely. In contrast, use of the normalized height alone may lead to an overestimation of Ti coordination number. Using both parameters, determination of Ti coordination number in oxide compounds is much more reliable and robust, even for mixtures of different Ti coordinations. It is possible, for example, to distinguish between fivefold coordinated Ti alone versus a 50:50 mixture of fourfold and sixfold coordinated Ti.

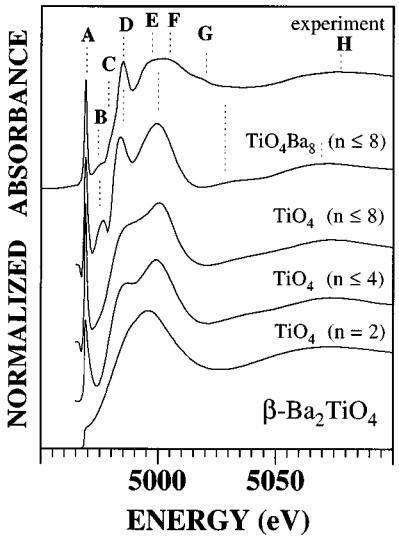

FIG. 7. Comparison of the experimental Ti K XANES spectrum for β-$Ba_2{}^{[4]}TiO_4$ with theoretical spectra from FEFF MS calculations on TiO_4 and TiO_4Ba_8 clusters. In the small cluster calculations, the TiO_4 unit was embedded in the larger cluster, which is representative of the medium-range environment around Ti in this crystal structure. Calculations for the TiO_4 units were done for $n=2$, $n\leqslant 4$, and $n\leqslant 8$, which represent the order of scattering paths considered. The calculation for the TiO_4Ba_8 cluster was for $n\leqslant 8$.

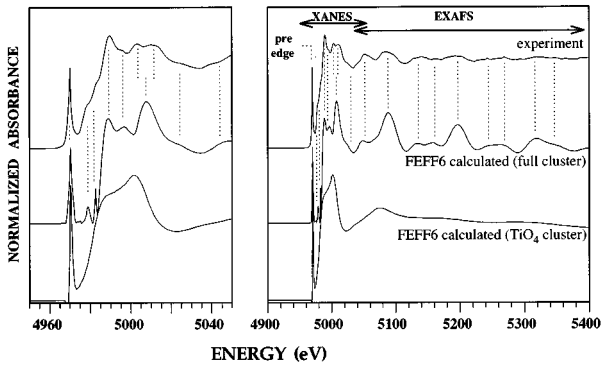

FIG. 8. Comparison of the experimental Ti K-edge XANES (left) and XANES+EXAFS spectrum (right) for $Ni_{2.6}{}^{[4]}Ti_{0.7}O_4$ spinel. Top: experimental spectrum; middle: theoretical spectrum ($n\leqslant 8$) calculated for a large cluster ($^{[4]}TiO_4Ni_{12}O_{12}Ti_4O_{12}Ni_{22}Ti_{12}$); bottom: theoretical spectrum ($n\leqslant 8$) calculated for a $^{[4]}TiO_4$ cluster embedded in the previous cluster.

V. Ti K-EDGE XANES CALCULATIONS FOR SELECTED MODEL COMPOUNDS

Ti K XANES spectra were modeled for β-$Ba_2{}^{[4]}TiO_4$ (Fig. 7), $Ni_{2.6}{}^{[4]}Ti_{0.7}O_4$ (Fig. 8), $K_2{}^{[5]}Ti_2O_5$ (Fig. 9), $Ba_2{}^{[5]}TiSi_2O_8$ (Fig. 10), and rutile (r-TiO_2; Fig. 11) using FEFF. Table II contains structural data used in calculating the XANES spectra presented here. Some authors have attributed the first main-edge feature (feature D in Fig. 7) to a $1s\rightarrow 4p$ transition and an associated shake-down effect.[1,9] Others, however, attribute these features to MS of the ejected photoelectron wave from the central absorbing atom to its nearest and next-nearest neighbors.[13–19] As discussed below,

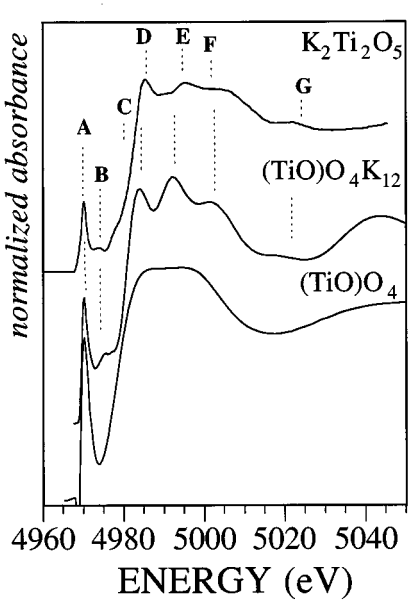

FIG. 9. Comparison of the experimental Ti K XANES spectrum of $K_2{}^{[5]}Ti_2O_5$ with theoretical spectra from FEFF calculations on $(^{[5]}TiO)O_4$ and $(^{[5]}TiO)O_4K_{12}$ clusters. As for the spinel, the $(^{[5]}TiO)O_4$ cluster calculation was carried out with the smaller cluster embedded in the larger K-containing cluster and with $n\leqslant 8$.

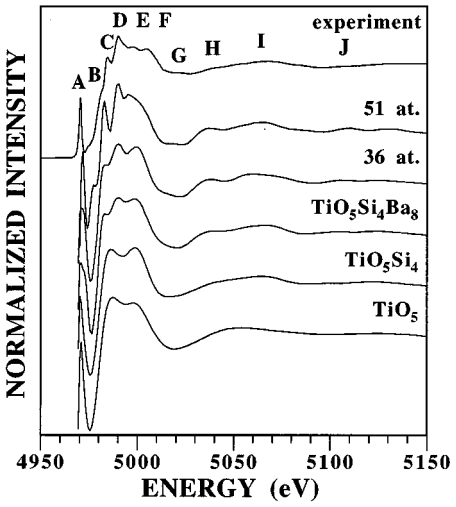

FIG. 10. *Ab initio* Ti *K*-edge XANES spectra calculated (using FEFF) for different clusters around Ti in crystalline $Ba_2TiSi_2O_8$ (from bottom to top): calculated spectra ($n \leqslant 8$) for several clusters: ($^{[5]}$Ti═O)O_4 (6 atoms), ($^{[5]}$Ti═O)O_4Si_4 (10 atoms), ($^{[5]}$Ti═O)$O_4Si_4Ba_8$ (18 atoms) and for two large clusters of atoms (containing 36 and 52 atoms, respectively) compared to experiment (top).

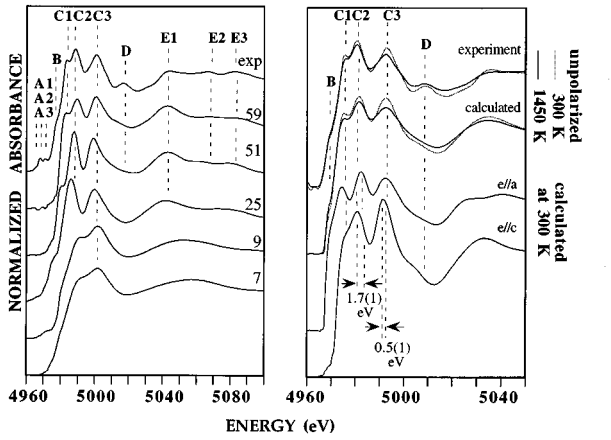

FIG. 11. Ti *K*-edge XANES spectra calculated for rutile. Left: XANES calculations for selected clusters around the absorbing Ti. Except for the pre-edge region, which requires a full MS calculation (Ref. 19), the XANES and EXAFS regions can be reproduced relatively well using only 59 atoms (cluster up to 5.5 Å from the central Ti). Note the presence of the three edge crests, including $C1$, which is related to high-order MS paths with an effective distance near 12.5 Å. The features are reproduced in position to within ± 0.7 eV of the experimental values. Right: Temperature (top four spectra) and polarization (bottom two spectra) dependences for rutile. Experimental scans (top two spectra) were collected at 300 (gray) and 1450 K (black) at SSRL using a high-temperature furnace working in the fluorescence detection mode. The calculated spectra (bottom four) reproduce the variation of $C1$ and $C2$ (among others) in intensity and position for different temperatures or polarizations. Experimental data and information for the polarization dependence of rutile at the Ti *K*-edge can be found elsewhere (Ref. 27).

these physical interpretations are not fully equivalent, and the results of the FEFF simulations verify quantitatively the validity of the MS viewpoint.

A. β-$Ba_2{}^{[4]}TiO_4$

The calculated Ti *K* XANES spectrum for β-$Ba_2{}^{[4]}TiO_4$ (using a 13-atom cluster, $^{[4]}TiO_4Ba_8$, derived from an x-ray crystal structure analysis;[20] see Table II) agrees well with that measured experimentally (Fig. 7). The two pre-edge features (A and B) are reproduced at the correct positions (within ± 1 eV of the experimental values). Feature C in the experimental spectrum is not clearly resolved in the calculated spectrum and appears to occur on the low-energy side of feature D in the calculated spectrum. Two main-edge features (D and E) are present in the calculated spectrum. In fact, in FEFF calculations for the same $^{[4]}TiO_4Ba_8$ cluster in which only the paths for the TiO_4 tetrahedron are considered (Fig. 7), feature D has a low height. In contrast, the second main-edge feature (E) is similar in both calculations and is due to single and MS involving principally the Ti-O pairs. The weak feature G is not reproduced in the calculated spectrum for a 13-atom cluster around Ti in β-$Ba_2{}^{[4]}TiO_4$.

Consideration of FEFF calculations for the TiO_4 cluster embedded in the larger TiO_4Ba_8 cluster using successively larger scattering orders ($n=2$, $n \leqslant 4$, $n \leqslant 8$) (Fig. 7) provides additional insight about the origin of the different edge features. Order $n=2$ corresponds to a Ti→O→Ti single scattering path in which the photoelectron leaves the central Ti, travels to a first-neighbor O, then is scattered back to the central Ti. Order $n=4$ corresponds to a MS path with up to four scattering legs along a Ti→O→Ti→O→Ti path within the tetrahedron (scattered two times by O first neighbors). Thus, the spectrum for orders $n \leqslant 4$ is the sum of the spectra for orders 2, 3, and 4. A calculation that contains MS paths up to order 8 for the larger Ba-containing cluster shows that the eight second-neighbor Ba atoms around the central Ti are responsible for feature B, and that they contribute significantly to the intensity of feature D. These calculations also show that the scattering path of order 2 contributes very little to the pre-edge feature, whereas the scattering paths of $n \leqslant 4$ and $n \leqslant 8$ give most of its intensity (especially, the 4-order path O⇄Ti⇄O).

B. $Ni_{2.6}{}^{[4]}Ti_{0.7}O_4$

This cation-excess spinel contains fourfold coordinated Ti.[21] Because FEFF calculations for TiO_4 units have already been discussed for β-Ba_2TiO_4 in the preceding section, only a few of the details will be discussed here. A large cluster of neighboring atoms (up to 78 atoms around the central Ti; Table II) was necessary to account for the numerous XANES features of $Ni_{2.6}{}^{[4]}Ti_{0.7}O_4$ (because of the high degree of symmetry around Ti in this $Fd3m$ structure[22]). The calculated spectrum is in excellent agreement with experiment (Fig. 8). Most of the XANES features are due to scattering from next-nearest neighbors, whereas the coordination sphere of Ti (TiO_4 cluster) contributes essentially only to the pre-edge. This calculation shows that combined *ab initio* XANES and EXAFS calculations can now be performed, which allows one to predict the full x-ray absorption fine structure spec-

TABLE II. Atomic clusters used for Ti *K*-edge XANES calculations.

β-$Ba_2^{[4]}TiO_4$		$Ni_{2.6}^{[4]}Ti_{0.7}O_4$		$K_2^{[5]}Ti_2O_5$		$Ba_2^{[5]}TiSi_2O_8$		r-$^{[6]}TiO_2$	
Pair	d (Å)	Pair	d (Å)	Pair	d (Å)	Pair	d (Å)	Pair	d (Å)
Ti—O	1.766	Ti—O	1.833 (×4)	Ti═O	1.585 (×1)	Ti═O	1.698 (×1)	Ti—O	1.95 (×4)
Ti—O	1.812	Ti—Ni	3.457 (×12)	Ti—O	1.906 (×1)	Ti—O	1.970 (×4)	Ti—O	1.98 (×2)
Ti—O	1.817	Ti—O	3.462 (×12)	Ti—O	1.988 (×2)	Ti—Si	3.357 (×4)	Ti—Ti	2.96 (×2)
Ti—O	1.836	Ti—Ti	3.611 (×4)	Ti—O	1.990 (×1)	Ti—O	3.513 (×1)	Ti—O	3.49 (×8)
Ti—Ba	3.148	Ti—O	4.525 (×12)	Ti—K	3.583 (×2)	Ti—O	3.780 (×4)	Ti—Ti	3.57 (×8)
Ti—Ba	3.373	Ti—Ni	4.544 (×12)	Ti—K	3.612 (×1)	Ti—Ba	3.976 (×4)	Ti—O	4.08 (×8)
Ti—Ba	3.434	Ti—Ni	5.416 (×10)	Ti—K	3.660 (×2)	Ti—Ba	4.211 (×4)	Ti—O	4.52 (×8)
Ti—Ba	3.554	Ti—Ti	5.896 (×12)	Ti—K	4.064 (×2)	Ti—Ti	5.210 (×2)	Ti—Ti	4.59 (×4)
Ti—Ba	3.578			Ti—K	5.208 (×1)	Ti—Si	5.446 (×4)	Ti—O	4.61 (×4)
Ti—Ba	3.634			Ti—K	5.243 (×2)	Ti—Ti	6.029 (×4)	Ti—O	5.40 (×8)
Ti—Ba	3.817			Ti—K	4.064 (×2)	Ti—Si	6.099 (×4)	Ti—Ti	5.46 (×8)
Ti—Ba	4.315					Ti—Si	6.296 (×4)	Ti—Ti	5.50 (×8)
Ti—Ba	4.600					Ti—Ba	6.400 (×4)		
						Ti—Ba	6.549 (×4)		
						Ti—Si	7.470 (×4)		

trum. Again, the amplitude discrepancies are due in large part to the neglect of Debye-Waller factors.

C. $K_2^{[5]}Ti_2O_5$

The theoretical spectrum generated for $K_2^{[5]}Ti_2O_5$ using an 18-atom cluster, $(TiO)O_4K_{12}$ with the same structure as in the bulk crystal,[22] shows good agreement with the observed spectrum (Fig. 9). Here again, the main *K*-edge peak intensity is due mainly to MS among nearest-neighbor oxygens, but MS involving second-neighbor K makes important contributions to features *B*, *D*, *E*, *F*, and *G*, which appear to be diagnostic of the presence of K in the second shell around Ti. Detailed examination of the FEFF calculation suggests that features *D*, *E*, and *F* are related to MS along triangular Ti→O→K→Ti paths in $K_2^{[5]}Ti_2O_5$. Also present in the calculated spectrum of $K_2^{[5]}Ti_2O_5$ is feature *G*, which is observed in the experimental spectrum. The path amplitudes generated by FEFF show that feature *G* is due to MS paths involving the more distant K ions in the 18-atom cluster.

D. $Ba_2^{[5]}TiSi_2O_8$

Ab initio XANES calculations were performed for this compound (known as ''fresnoite''), based on the crystal structure reported by Markgraf *et al.*[23] In the experimental spectrum, a large number of features can be observed (*A* through *I*, Fig. 10), similar to the spinel previously studied. In this compound, Ti(IV) is fivefold coordinated and located in a square pyramid environment with one short double Ti═O distance (called ''titanyl'' with a bond length of 1.70 ± 0.01 Å) and 4 longer Ti—O bonds (length of 1.97 ± 0.01 Å, Table II), forming a $(Ti{=}O)O_4$ polyhedron.[23] Using only the first oxygen neighbors around Ti, only the pre-edge feature (*A*), the two edge crests (*C* and *F*), and the first maximum of the EXAFS signal (*H* or *I*) are reproduced in the calculated XANES spectra. If the cluster is extended to the next shell of neighboring atoms around Ti (four Si and eight Ba: Table II), the general shape of the XANES is obtained (features *C*, *D*, *F*, and *G*) and the beginning of the EXAFS region is well predicted (*H* and *I*). However, the edge crest is not well reproduced in detail, especially the splitting between features *E* and *F*. That splitting can be obtained in the calculated spectrum by using a larger cluster around Ti (52 atoms), resulting in a calculated XANES spectrum that is closer to that measured experimentally. The cluster results in XAFS contributions arising mostly from Ba next-nearest neighbors at distances of up to 7.5 Å with smaller contributions from Si and Ti. The third-neighbor oxygens at distances above 5 Å from the central Ti contribute little to the XAFS spectrum. In this calculated XANES spectrum, some weak features are missing (such as, e.g., a small feature between features *D* and *E*), which is probably due to an insufficiently large cluster.

E. r-$^{[6]}TiO_2$ (rutile)

Rutile (r-TiO_2) has been the subject of numerous experimental and theoretical x-ray-absorption near-edge studies. The Ti *K* XANES spectrum of rutile is complex, with three predges (features $A1-A3$ in Fig. 11), and three edge crests (features $C1-C3$), which were relatively poorly predicted in past studies. Different explanations of the three pre-edges have been published; we will consider here only the most recent interpretations, excluding the earlier excitonic model for the first pre-edge feature.[24] Ruiz-López and co-workers[15] have interpreted these pre-edges by suggesting that the *p* orbitals of the absorbing Ti can be mixed with the *d* orbitals of the neighboring Ti atoms. In their view, the pre-edge feature is due to transitions to this mixed p-d orbital. Wu and co-workers[17] suggested that the first and second pre-edge features are due to dipolar transitions from Ti $1s$ to t_{2g} and e_g levels (first and second pre-edge). The third pre-edge feature is thought to represent a transition to $4p$ levels of the absorbing Ti. Based on experiment[25] and/or calculations,[16,19] other authors suggested that the first pre-edge may be due mostly to quadrupolar transitions to t_{2g} levels of the TiO_6 octahedron. In this model, the second pre-edge is attributed mostly to $1s$ to $3d$ dipolar transitions to the t_{2g} orbital of the

neighboring octahedra around the octahedron containing the absorbing atom. The third pre-edge is attributed to another dipolar transition to the e_g orbital of the neighboring octahedra.

The three edge crests have not been reproduced accurately,[18] particularly feature $C1$, except in the calculations of Aïfa and co-workers,[19] who succeeded in reproducing this feature using a 290-atom cluster and the XAFS-Rostock code[26] as well as those by Wu and co-workers[17] (feature labeled $D1$ in their work). Here, we present FEFF calculations using a smaller cluster (up to 59 atoms) from a recent crystal structure refinement of rutile,[27] which reproduce the XANES and the EXAFS regions. In our calculations for rutile, we found that MS contributions out to effective distances of 15 Å from the central atom are extremely important. Therefore, a very large number of paths (more than 5×10^6 on the average) have been taken into account (fortunately, due to the symmetry of rutile, this number degenerates to a few hundred thousand paths). As a result, the calculations presented here require large amounts of RAM ($\approx$100 Mbytes, at least) because some of the FEFF internal parameters need to be adjusted so that all paths up to 15 Å in effective distance are included (the most important parameter is nheap, which must be set to 2.5×10^6).

Figure 11 shows the results obtained for the pre-edge (left) and the XANES (right). A calculation involving only the TiO_6 octahedron reproduces only a portion of the third edge crest ($C3$). The second edge crest ($C2$) appears when O and Ti third neighbors (eight Ti and eight O at approximately the same distance, $\approx$3.56–3.57 Å from the central Ti) are included in the cluster. The first of the three edge crest ($C1$) does not appear until at least 59 atoms are included in the cluster (cluster diameter of 5.5 Å). Feature $C1$ is, therefore, related to the presence of O and Ti next-nearest neighbors around Ti (see Table II), which make significant MS contributions of order 4 with an effective distance between 11 and 13 Å. FEFF calculations not including such high effective distance contributions (i.e., those in which the FEFF default nheap parameter is used) cannot reproduce feature $C1$ (cf. Ref. 18).

The accuracy of these FEFF calculations can be further tested by examining the polarization and temperature dependence of these models in comparison with experiment (Fig. 11, right). When the electric field vector **e** of the incident x-ray beam is parallel to the **a** axis of the rutile crystal structure, features B and C are strongly enhanced relative to the unpolarized spectrum.[28] Also, the energy position of feature $C2$ is shifted to higher energies by $\approx$1 eV compared to the unpolarized spectrum. In contrast, features B and $C1$ are very weak and $C2$ is shifted toward lower energies when **e** is parallel to the **c** axis. We have measured Ti *K*-edge XANES spectra for rutile up to 1450 K.[4] Increasing temperature to 1450 K results in a relatively strong decrease in the intensities of features $C1$ and $C3$ relative to $C2$ (see Fig. 11, right, where $C1$ is no more than a shoulder at high temperature instead of an edge crest). These observed polarization and temperature dependences can be reproduced adequately using FEFF. For example, $C1$ is predicted to decrease in intensity when **e** is parallel to the c axis or when temperature increases, which is consistent with experiment. Also, using the same polarization setting, $C2$ is predicted to be shifted toward higher energies by $\approx1.65\pm0.09$ eV (when compared to **e**$\|$**a**), which is again consistent with experiment [the shift of $C2$ from **e**$\|$**c** to **e**$\|$**a** was observed to be 1.83 ± 0.08 eV (Ref. 28)].

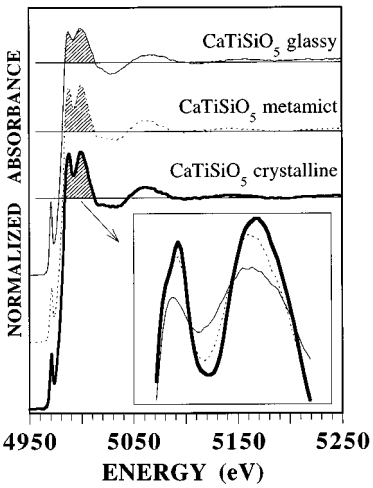

FIG. 12. Ti *K*-edge XANES spectra collected for various samples of $CaTiSiO_5$ (titanite) with variable degrees of aperiodicity: crystalline (solid lines), radiation-damaged (metamict) (dotted lines), and glassy (thick solid lines). The loss of long- and medium-range order broadens the edge crest significantly, while the pre-edge shifts to a position and a height that are typical of mixtures of sixfold and fivefold coordinated Ti. The insets show the overlapped edge crests in order to illustrate the absolute differences in intensities among the different samples studied.

VI. XANES AS A MEASURE OF MEDIUM-RANGE DISORDER

A. Effects of disorder on XANES

In general, the intensity of the dominant main-edge peak in ordered materials appears to be greater, relative to the edge jump, than in disordered materials of a given composition. The reason for this can be understood in terms of both the effects of disorder and the f-sum rule.[29] The f-sum rule implies that the total absorption integrated over all energies and absorption edges is a constant independent of the nature of the final state. Thus, disorder typically broadens spectra without altering the overall integrated strength. Two effects are important for the main edge in disordered materials. One is the statistical variation in edge position among various absorption sites due to disorder, i.e., the variation in the threshold E_0 in the absorption coefficient. This effect leads to a broadening of the EXAFS (which can be included by an additional imaginary part E_i to the potential), and can also have an appreciable effect at the edge. The second is the well-known Debye-Waller-like damping of the magnitude of the XAFS oscillations with respect to the smooth atomiclike background μ_0. This second effect is due to random phase decoherence among each set of closely similar MS paths, which in general [cf. the GNXAS interpretation of XAFS (Ref. 30)] gives each such set a Debye-Waller factor $\langle\exp(2ikR)\rangle=\exp[-W(k)]$. Here, R is the disorder-induced fluctuation in the effective or half-path length R for a given

N-leg path defined by position vectors $R_1, R_2, \ldots, R_N$, $W(k)$ is a generalized (usually complex) function, and the brackets refer to a configurational average. For large disorder, the function $W(k) = \Sigma_n (2k)^n \sigma^{(n)}/n!$ has substantial contributions from third and higher cumulants $\sigma^{(n)}$. This leads us to propose a principle of disorder-induced XANES broadening that also takes into account the variation of E_0 at the edge (which can be represented as a complex E_0) and is thus more general than Debye-Waller damping alone. A good illustration of this proposed principle is seen in the comparison of Ti K-edge XANES spectra for crystalline, radiation-damaged, and glassy $CaTiSiO_5$ (Fig. 12). Radiation-damaged $CaTiSiO_5$ is naturally occurring (''metamict titanite'') and is partially aperiodic because of alpha-recoil damage due to the decay of actinide elements (Th and U) over hundreds of millions of years.[31] Glassy $CaTiSiO_5$ is a fully aperiodic modification, quenched from an high-temperature melt. From Fig. 12, it can be seen that the Ti K-edge XANES features are narrower for crystalline $CaTiSiO_5$ compared to its radiation-damaged counterpart. The glassy $CaTiSiO_5$ sample shows the most broadened XANES features, which is consistent with a loss of periodicity in the medium-range structural region around Ti due to the glassy state. This correlation between the degree of medium-range structural order and the intensity of the main absorption edge is consistent with the above principle.

B. Application: XANES analysis of structural disorder around Ti in glassy and molten $K_2TiSi_2O_7$

An important application of the experimental and theoretical studies of Ti coordination environments in oxide compounds is to titanosilicate glasses and melts where the local environment of Ti is not well known and the presence of Ti is known to cause significant changes in physical properties such as viscosity and heat capacity. For example, recent studies[32] of the heat capacity of $K_2TiSi_2O_7$ glass near the glass transition temperature (T_g, between 500 and 1000 K) show positive anomalies that have been attributed to possible changes in Ti coordination number. *Ab initio* XANES calculations have been performed using atomic clusters constructed on the basis of EXAFS information for titanosilicate glasses and melts (collected up to 1650 K). These clusters were optimized using bond-valence theory. This strategy has been presented in another paper.[33] In this earlier study, we were able to detect third-neighbor alkali cations around Ti in the XANES spectra that were not detected in the EXAFS region. This strategy for probing disorder effects in the XANES region illustrates how a combination of experiment and theory can be used to constrain possible models for the local and medium-range structures around Ti in a titanosilicate glass/melt (see Ref. 33).

VII. SUMMARY AND CONCLUSIONS

In this study, we have presented high-resolution Ti K XANES spectra of several crystalline model compounds and have successfully modeled these spectra using the *ab initio* multiple-scattering code FEFF. This combination of experiment and theory has allowed us to develop a scattering-theoretic interpretation of the experimental spectra in terms of the types and numbers of atoms and scattering paths that contribute to each spectral feature. A major conclusion of this study is that a high-order MS calculation of XANES, using a finite number of paths, provides a quantitative description of Ti K XANES spectra, including the pre-edge region. Thus full MS calculations of XANES spectra are not always essential, although in certain cases (e.g., the Ti K pre-edge of rutile), they may be required. We have successfully tested these models using additional experimental data collected either on mixtures of different Ti coordinations or XANES data collected at different temperatures or as a function of polarization with respect to the **e** vector of the x-ray beam. An experimental protocol is presented for extracting coordination information from Ti pre-K-edge features. Specifically, both the pre-edge position and height must be considered in determining Ti coordination environments in oxide compounds. In addition, a specific protocol is presented for FEFF XANES calculations at the Ti K edge in these compounds. One crucial step in this protocol is limiting the number of low-amplitude paths in the XANES calculation beyond the original default recommended for calculations of EXAFS spectra. A comparison of band theory and molecular-orbital theory interpretations of Ti pre-edge spectral features is made, which illustrates their equivalence.

Application of these protocols to aperiodic titanosilicate compounds, including radiation-damaged materials, titanosilicate glasses, and high-temperature titanosilicate melts, showed that original structural information can be extracted from the XANES region even when this information may not be accessible in the EXAFS region. A method for estimating disorder from XANES spectra is presented and applied to $CaTiSiO_5$ in crystalline and radiation-damaged (aperiodic) forms. Manifestations of these disorder effects, beyond the normal Debye-Waller damping, are phase decoherence of the XANES from various scattering paths due to medium-range disorder and the need for an additional contribution to the mean free path.

ACKNOWLEDGMENTS

The authors are indebted to the staffs of LURE and SSRL for their help. This work was supported by U.S. NSF Grant No. EAR-9305028 (G.E.B.), U.S. DOE Grant No. DE-FG06-ER45415 (J.J.R.), and by the NSF-CNRS International Program (Grant INT-9116008; G.E.B. and G. Calas). SSRL is supported by DOE and NIH (including subcontract RR 01209 to J.J.R.). We also thank B. Ravel and E. Stern for helpful comments.

*Corresponding author.

[1] R. B. Greegor *et al.*, J. Non-Cryst. Solids **55**, 27 (1983).

[2] C. A. Yarker *et al.*, J. Non-Cryst. Solids **79**, 117 (1986); L. Cormier, P. H. Gaskell, G. Calas, and J. Zhao (unpublished).

[3] G. E. Brown, Jr., G. Calas, G. A. Waychunas, and J. Petiau, in *Spectroscopic Methods in Mineralogy and Geology*, Reviews In Mineralogy, edited by F. C. Hawthorne (Mineralogical Society of America, Washington, DC, 1988), Vol. 18, p. 431.
[4] F. Farges, G. E. Brown, Jr., and J. J. Rehr, Geochim. Cosmochim. Acta **60**, 3023 (1996); F. Farges *et al.*, *ibid.* **60**, 3039 (1996); **60**, 3055 (1996); F. Farges, and G. E. Brown, Jr., Geochim. Cosmochim. Acta (to be published).
[5] G. A. Waychunas, Am. Mineral. **72**, 89 (1987).
[6] A. Ankudinov and J. J. Rehr (unpublished).
[7] S. I. Zabinsky *et al.*, Phys. Rev. B **52**, 2995 (1995).
[8] L. A. Grunes, Phys. Rev. B **27**, 2111 (1983).
[9] R. A. Bair and W. A. Goddard, Phys. Rev. B **22**, 2767 (1980).
[10] B. Ravel and J. J. Rehr (unpublished).
[11] W. L. Schaich, Phys. Rev. B **8**, 4028 (1973).
[12] P. Behrens *et al.*, J. Chem. Soc. Commun. **1990**, 678 (1990).
[13] E. Paris, C. Romano, and Z. Wu, Physica B **208–209**, 351 (1995).
[14] F. W. Kutzler *et al.*, J. Chem. Phys. **73**, 3274 (1980); A. Bianconi, E. Fritsch, G. Calas, and J. Petiau, Phys. Rev. B **32**, 4292 (1985); A. Bianconi *et al.*, J. Phys. (France) Colloq. **46**, C9-101 (1985); C. R. Natoli, and M. Benfatto, *ibid.* **47**, C8-11 (1986).
[15] M. F. Ruiz-López and A. Muñoz-Pàez, J. Phys. Condens. Matter **3**, 8981 (1991).
[16] T. Uozumi *et al.*, Europhys. Lett. **18**, 85 (1992); M. A. Khan, A. Kotani, J.-C. Parlebas, J. Phys. Condens. Matter **3**, 1763 (1991); K. Okada and A. Kotani, J. Electron Spectrosc. Relat. Phenom. **62**, 131 (1993).
[17] Z. Y. Wu, G. Ouvrard, P. Gressier, and C. R. Natoli, J. Phys. (France) I (to be published).
[18] V. Jeanne-Rose, Y. AÎfa, and B. Poumellec, J. Phys. (France) I (to be published).
[19] Y. Aïfa *et al.*, J. Phys. (France) I (to be published).
[20] K. K. Wu and I. D. Brown, Acta Crystallogr. Sec. B **29**, 2009 (1973).
[21] G. A. Lager *et al.*, J. Appl. Crystallogr. **14**, 261 (1981).
[22] S. Andersson and A. D. Wadsley, Acta Chem. Scand. **15**, 663 (1974).
[23] S. A. Markgraf, A. Halliyal, A. S. Bhalla, and R. E. Newnham, Ferroelectrics **62**, 17 (1985).
[24] R. Brydson *et al.*, J. Phys. Condens. Matter **1**, 797 (1989).
[25] C. Brouder, J. Phys. Condens. Matter **2**, 701 (1989).
[26] R. V. Vedrinskii *et al.*, Phys. Status Solidi B **111**, 433 (1982).
[27] C. J. Howard, T. M. Sabine, and F. Dickson, Acta Crystallogr. Sec. B **47**, 462 (1991).
[28] B. Poumellec *et al.*, Phys. Status Solidi B **164**, 319 (1991).
[29] M. Altarelli, D. L. Dexter, and H. M. Nussenzveig, Phys. Rev. B **6**, 4502 (1972).
[30] A. Filipponi and A. DiCicco, Phys. Rev. B **52**, 15 122 (1995); **52**, 15 135 (1995).
[31] R. C. Ewing, W. J. Weber, and F. W. Clinard, Jr., Prog. Nucl. Energy **29**, 63 (1995).
[32] P. Richet and Y. Bottinga, Geochim. Cosmochim. Acta **49**, 471 (1985); R. A. Lange and A. Navrotsky, *ibid.* **57**, 3001 (1993).
[33] F. Farges *et al.*, Geochim. Cosmochim. Acta **60**, 3055 (1996).